

PAPER

## A computational study of steady and stagnating positive streamers in $N_2-O_2$ mixtures

To cite this article: Xiaoran Li *et al* 2022 *Plasma Sources Sci. Technol.* **31** 065011

View the [article online](#) for updates and enhancements.

### You may also like

- [On electric field measurements based on intensity ratio of 1 and 2<sup>nd</sup> systems of nitrogen in discharges with high specific deposited energy.](#)

Nikita D. Lepikhin, Nikolay A Popov and Svetlana M Starikovskaia

- [Progress in the development and construction of high temperature superconducting magnets](#)

H Yavari

- [Field Enhancement in Nanoparticles Due to IR Vortex Beams](#)

Sahil Sharma, Abhisek Sinha, Vandana Sharma *et al.*



# HIDEN ANALYTICAL

## Analysis Solutions for your Plasma Research

- Knowledge,
- Experience,
- Expertise

[Click to view our product catalogue](#)

Contact Hiden Analytical for further details:  
**W** [www.HidenAnalytical.com](http://www.HidenAnalytical.com)  
**E** [info@hiden.co.uk](mailto:info@hiden.co.uk)



**Surface Science**

- ▶ Surface Analysis
- ▶ SIMS
- ▶ 3D depth Profiling
- ▶ Nanometre depth resolution



**Plasma Diagnostics**

- ▶ Plasma characterisation
- ▶ Customised systems to suit plasma Configuration
- ▶ Mass and energy analysis of plasma ions
- ▶ Characterisation of neutrals and radicals

# A computational study of steady and stagnating positive streamers in $N_2-O_2$ mixtures

Xiaoran Li<sup>1,2</sup>, Baohong Guo<sup>1</sup>, Anbang Sun<sup>2</sup>, Ute Ebert<sup>1,3</sup> and Jannis Teunissen<sup>1,\*</sup>

<sup>1</sup> Centrum Wiskunde & Informatica, Amsterdam, The Netherlands

<sup>2</sup> State Key Laboratory of Electrical Insulation and Power Equipment, School of Electrical Engineering, Xi'an Jiaotong University, Xi'an, 710049, People's Republic of China

<sup>3</sup> Eindhoven University of Technology, Eindhoven, The Netherlands

E-mail: [jannis.teunissen@cw.nl](mailto:jannis.teunissen@cw.nl)

Received 21 January 2022, revised 23 May 2022

Accepted for publication 9 June 2022

Published 5 July 2022



CrossMark

## Abstract

In this paper, we address two main topics: steady propagation fields for positive streamers in air and streamer deceleration in fields below the steady propagation field. We generate constant-velocity positive streamers in air with an axisymmetric fluid model, by initially adjusting the applied voltage based on the streamer velocity. After an initial transient, we observe steady propagation for velocities of  $3 \times 10^4 \text{ m s}^{-1}$  to  $1.2 \times 10^5 \text{ m s}^{-1}$ , during which streamer properties and the background field do not change. This propagation mode is not fully stable, in the sense that a small change in streamer properties or background field eventually leads to acceleration or deceleration. An important finding is that faster streamers are able to propagate in significantly lower background fields than slower ones, indicating that there is no unique stability field. We relate the streamer radius, velocity, maximal electric field and background electric field to a characteristic time scale for the loss of conductivity. This relation is qualitatively confirmed by studying streamers in  $N_2-O_2$  mixtures with less oxygen than air. In such mixtures, steady streamers require lower background fields, due to a reduction in the attachment and recombination rates. We also study the deceleration of streamers, which is important to predict how far they can propagate in a low field. Stagnating streamers are simulated by applying a constant applied voltage. We show how the properties of these streamers relate to the steady cases, and present a phenomenological model with fitted coefficients that describes the evolution of the velocity and radius. Finally, we compare the lengths of the stagnated streamers with predictions based on the conventional stability field.

Keywords: stability field, steady streamers, stagnating streamers

(Some figures may appear in colour only in the online journal)

## 1. Introduction

Streamer discharges [1, 2] are a common initial stage of electrical discharges, playing an important role for electric breakdown in nature and in high voltage technology. As a cold atmospheric plasma [3] they also have wide industrial applications [4–6]. The goal of this paper is to better understand positive

streamer propagation in air. In particular, we study when such streamers accelerate or decelerate in homogeneous fields, by locating the unstable boundary between these regimes with numerical simulations.

An important empirical concept for streamer propagation has been the ‘stability field’  $E_{st}$  [7], which is often defined as the minimal background electric field that can sustain streamer propagation. Experimentally, stability fields have been

\* Author to whom any correspondence should be addressed.

**Table 1.** Reactions included in the model, with reaction rates and references.  $E/N$  is the reduced electric field in Townsends. The electron temperature  $T_e$  in reaction rates  $k_{14}$  and  $k_{15}$  is obtained from the mean electron energy ( $\epsilon_e$ ) computed by BOLSIG+ as  $T_e = 2\epsilon_e/3k_B$ .

Reaction No.	Reaction	Reaction rate coefficient	Reference
1	$e + N_2 \xrightarrow{k_1} e + e + N_2^+ (15.60 \text{ eV})$	$k_1(E/N)$	[33, 32]
2	$e + N_2 \xrightarrow{k_2} e + e + N_2^+ (18.80 \text{ eV})$	$k_2(E/N)$	[33, 32]
3	$e + O_2 \xrightarrow{k_3} e + e + O_2^+$	$k_3(E/N)$	[33, 32]
4	$e + O_2 + O_2 \xrightarrow{k_4} O_2^- + O_2$	$k_4(E/N)$	[33, 32]
5	$e + O_2 \xrightarrow{k_5} O^- + O$	$k_5(E/N)$	[33, 32]
6	$O_2^- + N_2 \xrightarrow{k_6} O_2 + N_2 + e$	$k_6 = 1.13 \times 10^{-25} \text{ m}^3 \text{ s}^{-1}$	[38]
7	$O_2^- + O_2 \xrightarrow{k_7} O_2 + O_2 + e$	$k_7 = 2.2 \times 10^{-24} \text{ m}^3 \text{ s}^{-1}$	[38]
8	$O^- + N_2 \xrightarrow{k_8} e + N_2O$	$k_8 = 1.16 \times 10^{-18} \exp(-(\frac{48.9}{11+E/N})^2) \text{ m}^3 \text{ s}^{-1}$	[39]
9	$O^- + O_2 \xrightarrow{k_9} O_2^- + O$	$k_9 = 6.96 \times 10^{-17} \exp(-(\frac{198}{5.6+E/N})^2) \text{ m}^3 \text{ s}^{-1}$	[39]
10	$O^- + O_2 + M \xrightarrow{k_{10}} O_3^- + M$	$k_{10} = 1.1 \times 10^{-42} \exp(-(\frac{E/N}{65})^2) \text{ m}^6 \text{ s}^{-1}$	[39]
11	$N_2^+ + N_2 + M \xrightarrow{k_{11}} N_4^+ + M$	$k_{11} = 5 \times 10^{-41} \text{ m}^6 \text{ s}^{-1}$	[40]
12	$N_4^+ + O_2 \xrightarrow{k_{12}} O_2^+ + N_2 + N_2$	$k_{12} = 2.5 \times 10^{-16} \text{ m}^3 \text{ s}^{-1}$	[40]
13	$O_2^+ + O_2 + M \xrightarrow{k_{13}} O_4^+ + M$	$k_{13} = 2.4 \times 10^{-42} \text{ m}^6 \text{ s}^{-1}$	[40]
14	$e + O_4^+ \xrightarrow{k_{14}} O_2 + O_2$	$k_{14}(E/N) = 1.4 \times 10^{-12} (300 \text{ K}/T_e)^{1/2} \text{ m}^3 \text{ s}^{-1}$	[38]
15	$e + N_4^+ \xrightarrow{k_{15}} N_2 + N_2$	$k_{15}(E/N) = 2.0 \times 10^{-12} (300 \text{ K}/T_e)^{1/2} \text{ m}^3 \text{ s}^{-1}$	[38]

extensively investigated [8–13]. For positive streamers in air with standard humidity ( $11 \text{ g m}^{-3}$ ), reported values range from  $4.1$  to  $6 \text{ kV cm}^{-1}$ , with values around  $5 \text{ kV cm}^{-1}$  being the most common. Note that if there are multiple streamers, they will modify the background field in which each of them propagates. However, the small spread in experimental measurements indicates that the concept of a stability field nevertheless remains useful.

In [7, 8] it was suggested that a streamer would propagate with a constant velocity and radius in the stability field. This led to the concept of a ‘steady propagation field’ in which streamer properties like velocity and radius do not change [14, 15]. Such steady propagation was recently observed in numerical simulations in air in a field of about  $4.7 \text{ kV cm}^{-1}$  [15]. In these simulations, the conductivity behind the streamer head was lost after a certain length due to electron attachment and recombination. The resulting discharge resembled the minimal streamers found in [16]. Qin *et al* [14] proposed that steady propagation fields in air depend on streamer properties and that they could be as high as the breakdown electric field ( $28.7 \text{ kV cm}^{-1}$ ), based on energy conservation criteria [17].

In this paper, we address two main topics. The first is to study steady propagation fields for positive streamers in air, in particular the range of such fields and their dependence on streamer properties. The second topic is how streamers decelerate in fields lower than their steady propagation field, and whether the lengths of such streamers can be predicted.

Below, we briefly summarize some of the past work on decelerating and stagnating streamers. Pancheshnyi *et al* [18] numerically investigated the stagnation dynamics of positive streamers with an axisymmetric fluid model. It was shown that the streamer’s radius decreased as it decelerated, which led to a rapid increase in the electric field at the streamer head. More

recently, Starikovskiy *et al* [19] studied decelerating streamers in an inhomogeneous gas density with an axisymmetric fluid model. Among other things, the authors demonstrated the rather different stagnation dynamics of positive and negative streamers. In [15], it was observed that positive streamers decelerate and eventually stagnate in a background electric field below their steady propagation field. With a standard fluid model with the local field approximation, the electric field at the streamer head diverges as the streamer stagnates. In [20], suitable models for simulating positive streamer stagnation were investigated, and it was shown that the field divergence can be avoided by using an extended fluid model. We instead modify the impact ionization source term to avoid this unphysical divergence [21, 22].

In this paper, we also study the relation between the properties of steady streamers. Several relations have been found in past studies, in particular between the streamer velocity and radius. In the experimental work of Briels *et al* [16], the velocity  $v$  was parameterized in terms of the diameter  $d$  as  $v = 0.5d^2 \text{ mm}^{-1} \text{ ns}^{-1}$ , for both positive and negative streamers in an inhomogeneous field. In contrast, simulation results in [23] indicated an approximately linear relation between streamer velocity and radius for accelerating streamers. Approximate analytic results in [24] supported this quasi-linear relation, and it was shown that with certain assumptions, the maximum electric field at the streamer head can be determined from  $v$  and  $d$ .

We simulate the propagation of positive streamers in air with a 2D axisymmetric fluid model, which is described in section 2. In section 3, we investigate the properties of steady streamers, which are obtained by adjusting the applied voltage based on the streamer velocity. Afterwards, the deceleration

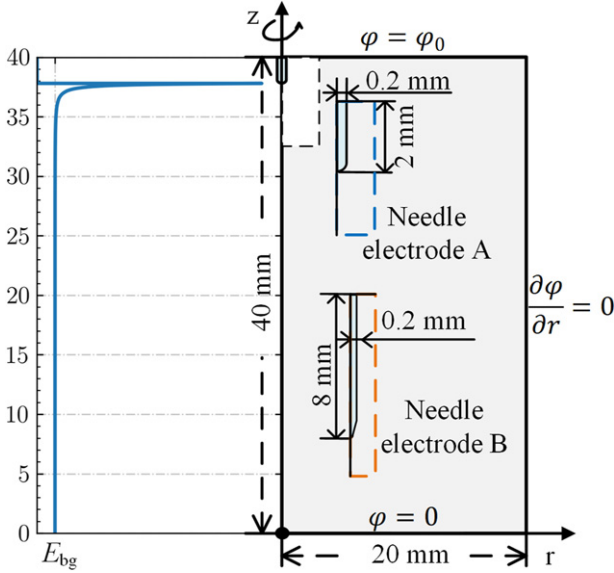


**Figure 1.** The computational domain. Right: electrode geometry and boundary conditions. The needle protrusions used for generating constant-velocity (needle electrode A) and stagnating streamers (needle electrode B) are illustrated. Left: axial electric field distribution with the 2 mm long needle.  $E_{bg}$  is the average electric field between the plate electrodes.

of streamers is studied, by simulating stagnating streamers in a low background field in section 4.

## 2. Simulation model

### 2.1. Fluid model and chemical reactions

We use a 2D axisymmetric drift–diffusion–reaction type fluid model with the local field approximation, as implemented in the open-source Afivo-streamer [25] code. For a recent comparison of experiments and simulations using Afivo-streamer see [26], and for a comparison between Afivo-streamer and five other simulation codes see [27]. Furthermore, in [28], simulations with fluid model used here were compared against particle-in-cell simulations in 2D and 3D, generally finding good agreement.

In the model, both electron and ion densities evolve due to transport and reaction terms. The temporal evolution of the electron density ( $n_e$ ) is given by

$$\partial_t n_e = \nabla \cdot (n_e \mu_e \mathbf{E} + D_e \nabla n_e) + S, \quad (1)$$

where  $\mu_e$  is the electron mobility,  $\mathbf{E}$  the electric field,  $D_e$  the electron diffusion coefficient and  $S$  is the sum of source terms, given by

$$S = f_\varepsilon S_i - S_\eta + S_{\text{detach}} - S_{\text{recom}} + S_{\text{ph}}, \quad (2)$$

where  $S_i$ ,  $S_\eta$ ,  $S_{\text{detach}}$ ,  $S_{\text{recom}}$  and  $S_{\text{ph}}$  are the source terms for impact ionization, attachment, detachment, electron–ion recombination and non-local photoionization, respectively, and  $f_\varepsilon$  is a correction factor discussed below. Photoionization is computed according to Zheleznyak’s model [29] using the

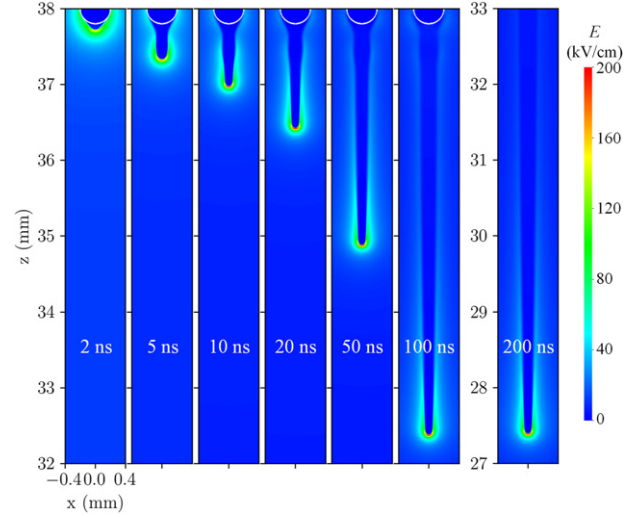


**Figure 2.** Electric field strength between 2 ns and 200 ns for a streamer whose velocity is forced to  $5 \times 10^4 \text{ m s}^{-1}$  by the velocity control method described in section 2.3. Note that the rightmost sub-figure has a different  $z$  axis. The white curves indicate the tip of the needle electrode.

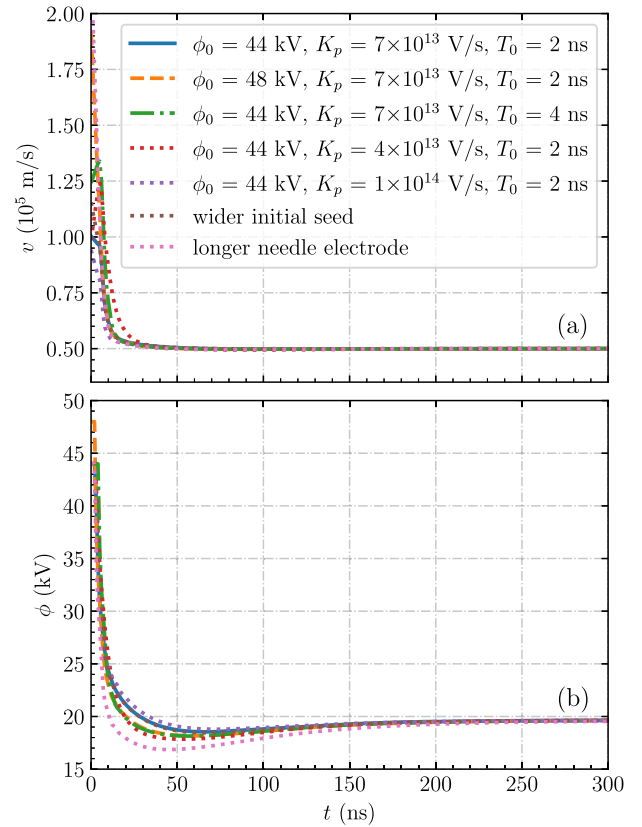


**Figure 3.** The streamer velocity (a) and applied voltage (b) versus time for streamers whose velocities are forced to be  $5 \times 10^4 \text{ m s}^{-1}$ . The initially applied voltage  $\phi_0$ , the start time of voltage adjustment  $T_0$  and the coefficient  $K_p$  in the velocity control method are varied. The cases labeled ‘wider initial seed’ and ‘longer needle electrode’ correspond to a  $R = 2 \text{ mm}$  initial Gaussian seed and a 2.5 mm long needle electrode. For these two cases,  $\phi_0 = 44 \text{ kV}$ ,  $T_0 = 2 \text{ ns}$ , and  $K_p = 7 \times 10^{13} \text{ V s}^{-1}$ .

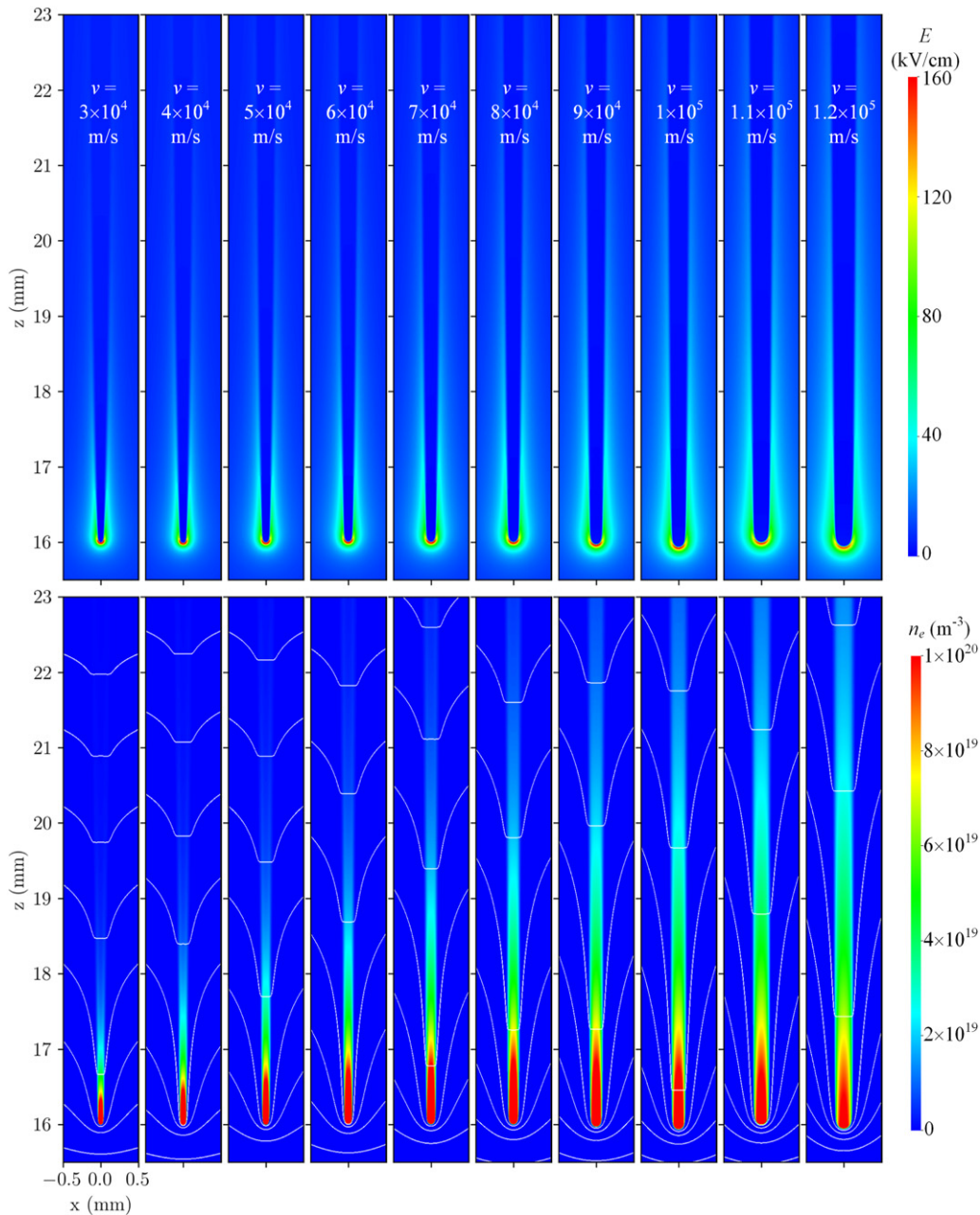


**Figure 4.** The electric field strength and the electron density for streamers in air at velocities of  $3 \times 10^4$  m s<sup>-1</sup> to  $1.2 \times 10^5$  m s<sup>-1</sup>, when their heads are at  $z = 16$  mm. All these streamers have reached steady states. The white equipotential lines are spaced by 0.5 kV. Behind the streamer heads, the radius increases due to ion motion.

Helmholtz approximation [30, 31], using the same photoionization model as [15].

The chemical reactions considered in this paper are listed in table 1. They include electron impact ionization ( $k_1$ – $k_3$ ), electron attachment ( $k_4$ ,  $k_5$ ), electron detachment ( $k_6$ – $k_8$ ), ion conversion ( $k_9$ – $k_{13}$ ) and electron–ion recombination ( $k_{14}$ ,  $k_{15}$ ). The electron transport data and the electron impact reaction coefficients depend on the reduced electric field  $E/N$ , and they were computed using BOLSIG+ [32] with Phelps’ cross sections for ( $N_2$ ,  $O_2$ ) [33, 34] using a temporal growth model. As was pointed out in [28], data computed with a temporal growth model is more suitable for positive streamer

simulations than data computed with a spatial growth model, which was used in [15].

Our model includes ion motion, which can be important at relatively low streamer velocities or when studying streamer stagnation [20]. The temporal evolution of each of the ion species  $n_j$  listed in table 1 is described by

$$\partial_t n_j = -\nabla \cdot (\pm n_j \mu_{\text{ion}} \mathbf{E}) + S_j, \quad (3)$$

where  $S_j$  is the sum of source terms for these species,  $\mu_{\text{ion}}$  is the ion mobility, and  $\pm$  is the sign of the species’ charge. For simplicity, we use a constant ion mobility  $\mu_{\text{ion}} = 2.2 \times 10^{-4}$  m<sup>2</sup> V<sup>-1</sup> s<sup>-1</sup> [35] for all ion species, as was also done in [15].

The electric field  $\mathbf{E}$  is computed as  $\mathbf{E} = -\nabla\varphi$  after solving Poisson's equation

$$\nabla \cdot (\varepsilon_0 \nabla \varphi) = -\rho, \quad (4)$$

where  $\varepsilon_0$  is the vacuum permittivity and  $\rho$  is the space charge density.

It can be difficult to simulate slow or stagnating positive streamers with a standard fluid model using the local field approximation [20]. Such streamers have a small radius, leading to strong electron density and field gradients that reduce the validity of the local field approximation [36, 37]. In [15, 18, 19] the electric field at the streamer tip was found to rapidly increase during streamer stagnation, and simulations had to be stopped after the field became unphysically large. Recently, it was shown that such unphysical behavior can be avoided by using an extended fluid model that includes a source term correction depending on  $\nabla n_e$  [20]. In this paper, we instead use a correction factor  $f_\epsilon$  for the impact ionization term as described in [21, 22]. This factor is given by

$$f_\epsilon = 1 - \frac{\hat{\mathbf{E}} \cdot \mathbf{\Gamma}^{\text{diff}}}{\|\mathbf{\Gamma}^{\text{drift}}\|}, \quad (5)$$

where  $\hat{\mathbf{E}}$  is the electric field unit vector, and  $\mathbf{\Gamma}^{\text{diff}}$  and  $\mathbf{\Gamma}^{\text{drift}}$  are the diffusive and drift flux of electrons, respectively, and  $f_\epsilon$  is limited to the range of [0, 1]. As discussed in [21, 22], this correction factor prevents unphysical growth of the plasma near strong density and field gradients. The underlying idea is that the diffusive electron flux parallel to the electric field (thus corresponding to a loss of energy) should not contribute to impact ionization.

## 2.2. Computational domain and initial conditions

We simulate positive streamers in  $\text{N}_2\text{-O}_2$  mixtures at 300 K and 1 bar, using the axisymmetric computational domain illustrated in figure 1. A high voltage is applied to the upper plate electrode (at  $z = 40$  mm), which includes a needle protrusion. The needle protrusion is implemented by modifying the multigrid methods in [41] using a level-set function, as described in [42]. For the constant-velocity streamers simulated in section 3, this needle is 2 mm long, with a radius of 0.2 mm and a semispherical tip. To generate the stagnating streamers simulated in section 4, more field enhancement is required. The needle used there is 8 mm long, with a radius of 0.2 mm, a conical tip with  $60^\circ$  top angle and a tip curvature radius of  $50 \mu\text{m}$ . The lower plate electrode (at  $z = 0$  mm) is grounded. A homogeneous Neumann boundary condition is applied for the electric potential on the radial boundary. For plasma species densities, homogeneous Neumann boundary conditions are used on all the domain boundaries. However, at the positive high-voltage electrode electron fluxes are absorbed but not emitted.

With the short needle electrode the axial electric field is approximately uniform, except for a small area around the needle tip, as shown in figure 1. For  $z$  between 0 mm and 32 mm, the electric field differs less than 1% from the average electric field between the plates  $E_{\text{bg}}$ . We therefore refer to  $E_{\text{bg}}$  as ‘the background electric field’ in the rest of the paper.

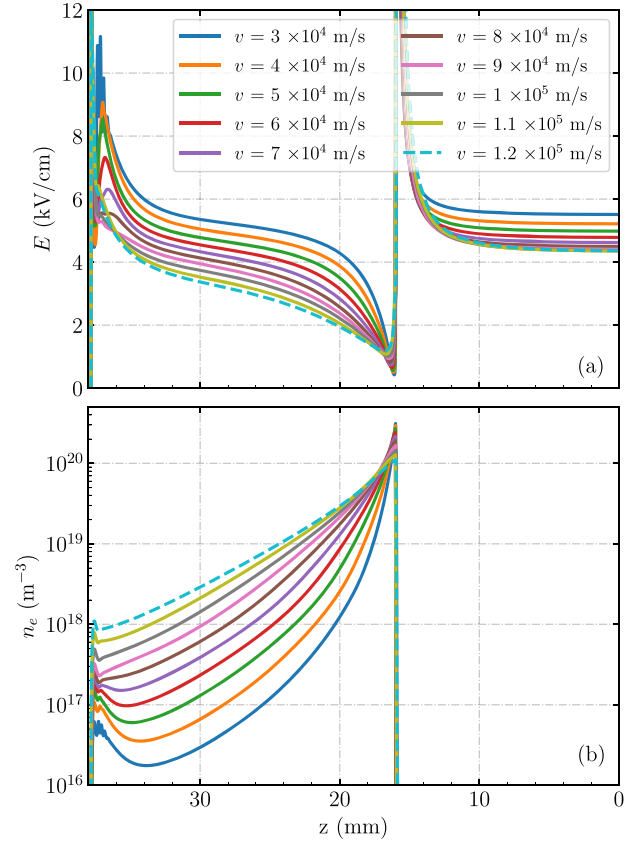


**Figure 5.** The axial electric field strength (a) and electron density (b) corresponding to figure 4.

To initiate the discharges, a neutral Gaussian seed consisting of electrons and positive ions ( $\text{N}_2^+$ ) is used. Its density is given by  $n_0 \exp(-(d/R)^2)$ , with  $n_0 = 10^{15} \text{m}^{-3}$ ,  $d$  the distance to the needle tip and  $R = 0.5$  mm. Besides this initial seed, no other initial ionization is included.

Adaptive mesh refinement is used in the model for computational efficiency. The refinement criterion for the grid spacing  $\Delta x$  is based on  $1/\alpha(E)$ , where  $\alpha(E)$  is the field-dependent ionization coefficient. If  $\Delta x > c_0 c_1 / \alpha(c_1 E)$ , the mesh is refined, and if  $\Delta x < \min\{0.125 c_0 c_1 / \alpha(c_1 E), d_0\}$ , the mesh is de-refined. We use  $c_0 = 0.5$ ,  $c_1 = 1.25$  and  $d_0 = 10 \mu\text{m}$ , which leads to a minimal grid spacing of  $\Delta x_{\text{min}} = 1.4 \mu\text{m}$ . Here  $c_1$  is used to balance the refinement ahead and on the sides of the streamer.

## 2.3. Velocity control method

In this paper, we study steady streamers propagating at a constant velocity. To generate such streamers, we adjust the applied voltage  $\phi$  based on the difference between the present streamer velocity  $v$  and a goal velocity  $v_{\text{goal}}$ . In the simulations, we cannot accurately measure  $v$  at every time step. Instead, we take samples  $v^*$  after the streamer head has moved more than  $8\Delta x_{\text{min}}$

$$v^* = (z_{\text{head}}^i - z_{\text{head}}^{i-1}) / (t^i - t^{i-1}),$$

where  $z_{\text{head}}$  is the location of the maximum electric field and the superscripts  $i$  and  $i - 1$  indicate the present and previous

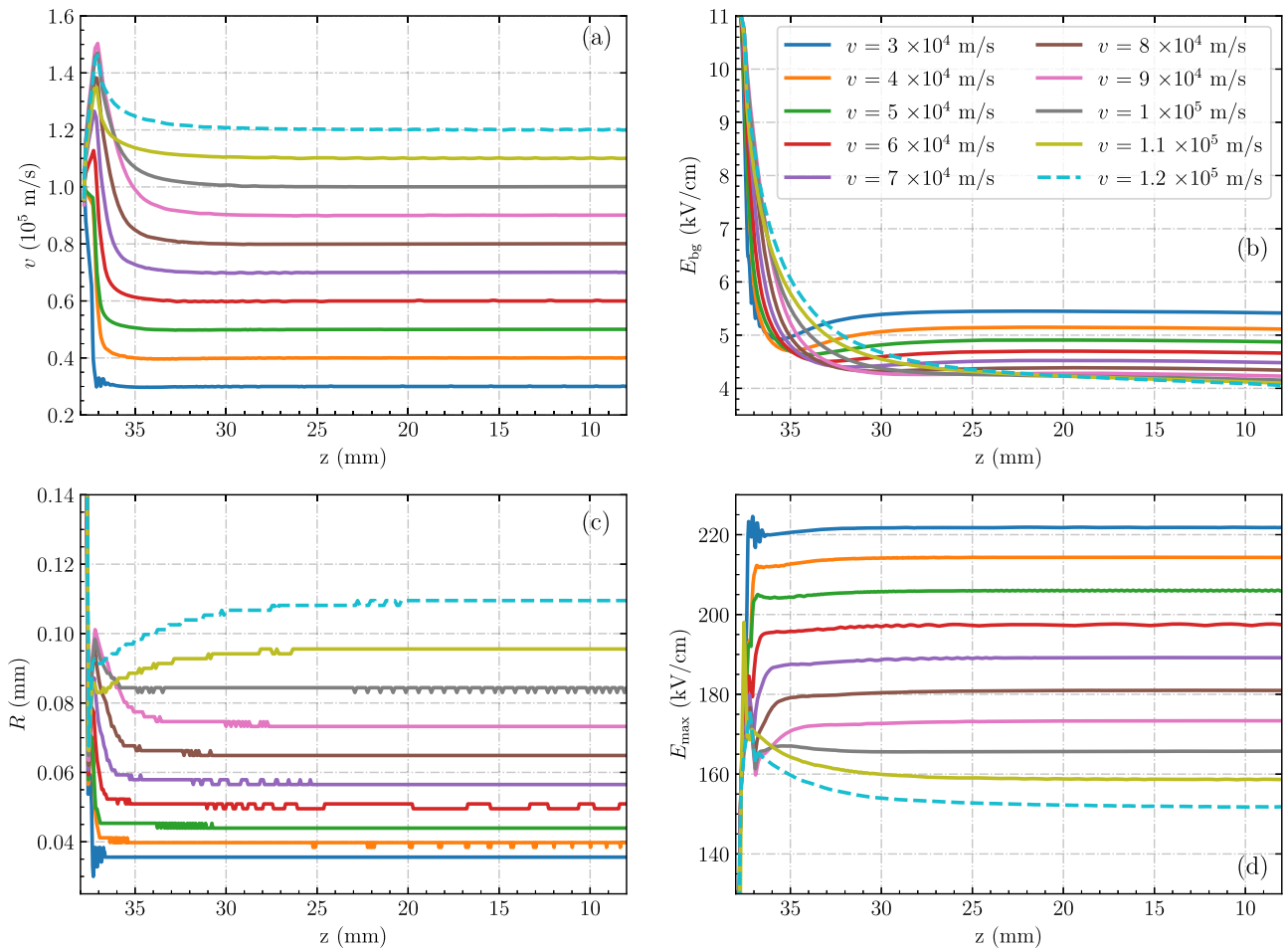


**Figure 6.** Streamer velocity (a), background electric field (b), streamer radius (c) and the maximal electric field (d) versus the vertical position of the streamer head for streamers in air at velocities from  $3 \times 10^4 \text{ m s}^{-1}$  to  $1.2 \times 10^5 \text{ m s}^{-1}$ . We take the location of the maximal electric field as the streamer head position, and the radius as the radial coordinate at which the radial electric field has a maximum. The thinnest (and slowest) streamer has a radius of around  $35 \mu\text{m}$ .

sampling time. Since this estimate is still rather noisy, we average it with the four most recent samples of  $v$  to obtain a smoothed velocity  $v^i$ . The voltage is then updated as

$$\phi^i = \phi^{i-1} + K_p(t^i - t^{i-1})(1 - v^i/v_{\text{goal}}), \quad (6)$$

where  $K_p$  is a proportionality constant between  $5 \times 10^{13} \text{ V s}^{-1}$  and  $2 \times 10^{14} \text{ V s}^{-1}$ .

Figure 2 shows an example of a streamer forced to propagate at  $5 \times 10^4 \text{ m s}^{-1}$ . Corresponding profiles for the streamer velocity and applied voltage are shown in figure 3 (the solid line). Initially, the applied voltage is 44 kV, which corresponds to a background electric field of  $11 \text{ kV cm}^{-1}$ . The applied voltage is adjusted after 2 ns, using  $K_p = 7 \times 10^{13} \text{ V s}^{-1}$ . As the applied voltage is reduced, the streamer velocity decreases, until it eventually converges to the goal velocity after about 50 ns. The applied voltage then slightly increases, until it stabilizes after about 200 ns.

The initially applied voltage ( $\phi_0$ ), the delay until the voltage is first adjusted ( $T_0$ ) and the coefficient  $K_p$  can affect how the streamer velocity approaches the goal value. Figure 3 shows the streamer velocities (a) and applied voltages (b) versus time for streamers whose velocities are forced to be  $5 \times 10^4 \text{ m s}^{-1}$

but with different  $\phi_0$ ,  $T_0$  and  $K_p$ . (Note that in the rest of the paper we will use  $\phi_0 = 44 \text{ kV}$ ,  $T_0 = 2 \text{ ns}$ , and  $K_p = 7 \times 10^{13} \text{ V s}^{-1}$ , unless stated otherwise.) Although the initial profiles vary, they eventually converge to the same value, which is also true for the streamer radius and the maximal electric field (which are not shown here). Two additional cases are included in figure 3. One is with a wider initial seed ( $R = 2 \text{ mm}$ ), and the other is with a longer needle electrode (2.5 mm). As shown in figure 3, the corresponding applied voltages converge to the same value. These examples therefore suggest that there is a unique propagation mode for a given constant streamer velocity. We have observed that for a steady streamer the charge profile near the streamer head translates with the streamer velocity, so that it remains constant.

### 3. Investigation of steady streamers

In this section, we investigate ‘steady streamers’ at constant velocities. We remark that these streamers are not actually stable, in the sense that a small change in their properties would lead to either acceleration or deceleration, as shown in appendix A. The streamers studied here thus

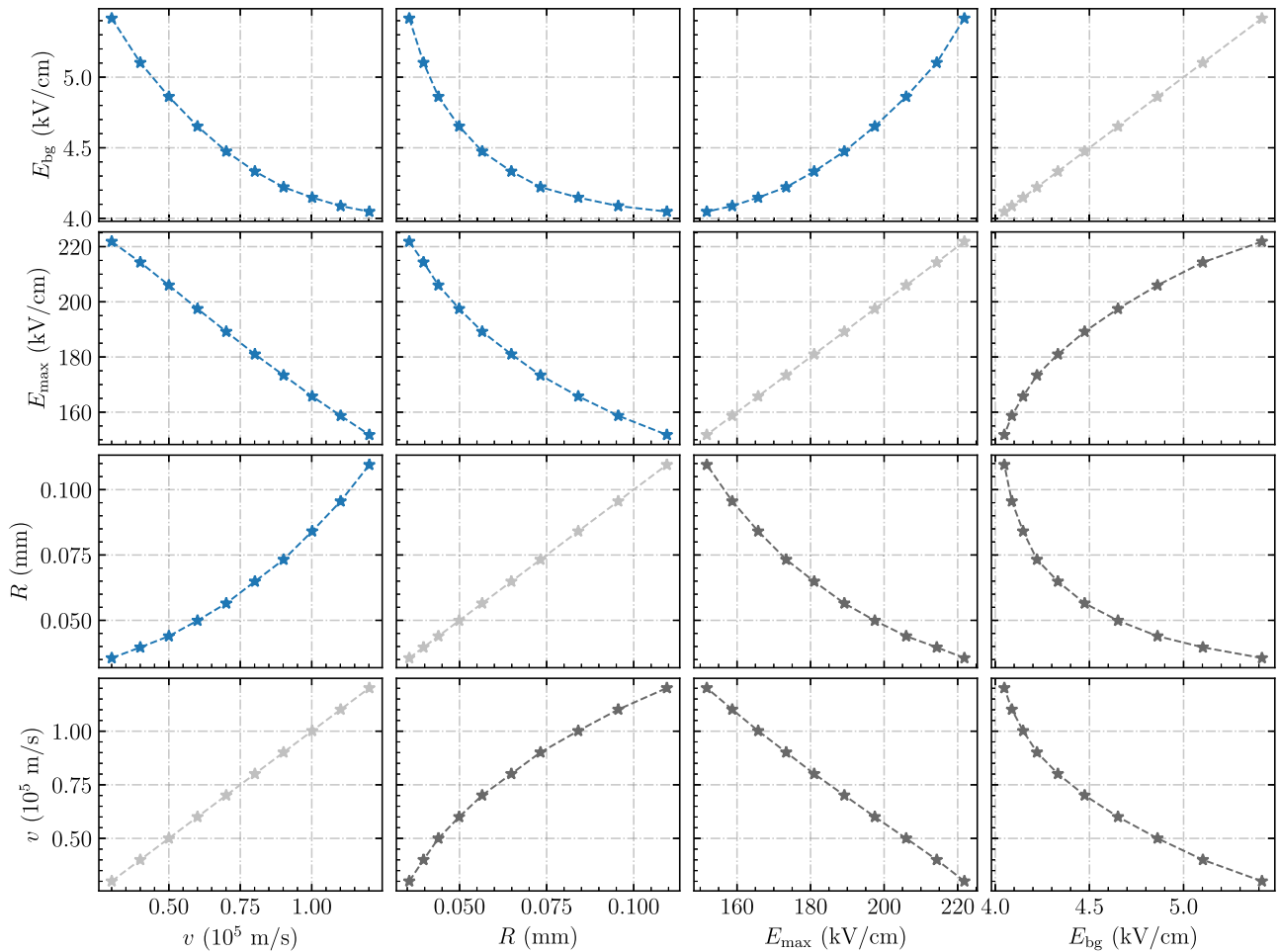


**Figure 7.** Overview of steady streamer properties. The blue curves show streamer velocity  $v$ , streamer radius  $R$ , maximum electric field  $E_{max}$  and background electric field  $E_{bg}$ . Each star symbol represents a steady propagation state, by taking the average over the last 30 ns of propagation. The picture shows each variable as a function of each other variable, with rows sharing the same y-axis and columns the same x-axis.

demarcate the unstable boundary between acceleration and deceleration.

### 3.1. Background electric fields for steady streamers with different velocities

We simulate streamers at constant velocities from  $3 \times 10^4$  m  $s^{-1}$  to  $1.2 \times 10^5$  m  $s^{-1}$ , using the velocity control method described in section 2.3. For the two slowest and two fastest streamers, we use  $K_p = 5 \times 10^{13}$  V  $s^{-1}$  and  $2 \times 10^{14}$  V  $s^{-1}$ , respectively. For the streamer at a velocity of  $1 \times 10^5$  m  $s^{-1}$ ,  $K_p = 1 \times 10^{14}$  V  $s^{-1}$  is used. A larger  $K_p$  is used for faster streamers so that it takes a similar distance for all streamers to enter a steady propagation mode. Figure 4 shows the electric field and the electron density for these streamers when their heads are at  $z = 16$  mm, and corresponding on-axis curves are shown in figure 5. Furthermore, figure 6 shows the evolution of the streamer velocity ( $v$ ), radius ( $R$ ), maximal electric field ( $E_{max}$ ) and the background electric field ( $E_{bg}$ ) versus streamer head position. The streamer radius is here defined as the radial coordinate at which the radial electric field has a maximum. We remark that there are other definitions of the streamer radius, such as the optical radius and the

electrodynamic radius [43], which would lead to a different value. When the streamers reach steady states,  $v$ ,  $R$ ,  $E_{max}$  and  $E_{bg}$  all remain constant. The values corresponding to these steady states are shown versus each other in figure 7.

Faster steady streamers have a larger radius and a lower maximal electric field, but they require a lower background electric field. For streamer velocities from  $3 \times 10^4$  m  $s^{-1}$  to  $1.2 \times 10^5$  m  $s^{-1}$  the corresponding background electric fields decrease from  $5.4$  kV  $cm^{-1}$  to  $4.1$  kV  $cm^{-1}$ . This dependence might at first seem surprising, but can be explained by considering the loss of conductivity in the streamer channel. Behind the streamer head, electron densities decrease due to attachment and recombination, and the electric field relaxes back to the background electric field [15]. This suggests we can define an effective streamer length as  $L_{eff} = v\tau$ , over which the background electric field is screened, where  $\tau$  is a typical time scale for the loss of conductivity. A faster streamer thus has a longer effective length, as can be seen in figure 5. A lower background electric field is therefore sufficient to get a similar amount of electric field enhancement. That streamers can have a finite conducting length was recently also observed in [15].

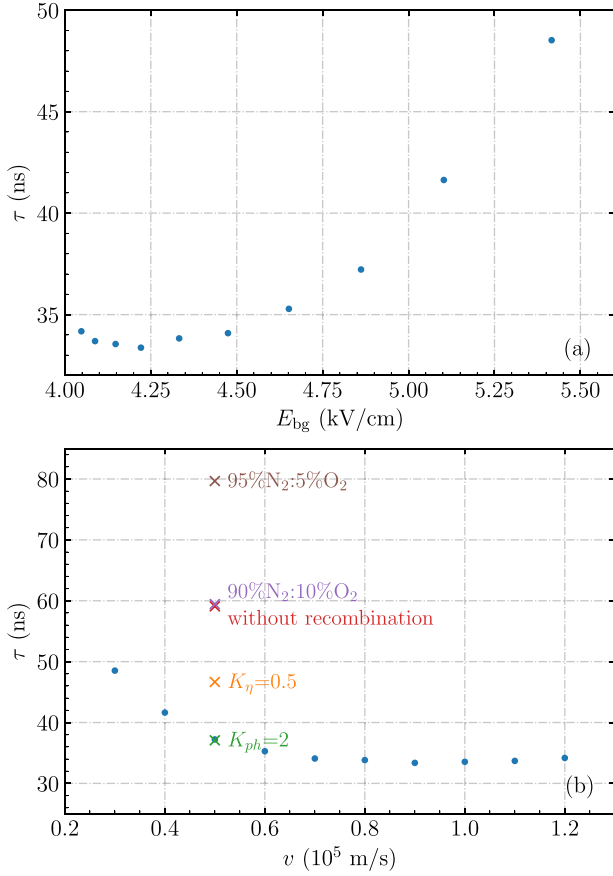


**Figure 8.** The time scale  $\tau$  given by equation (9) versus the background electric field (a) and versus the streamer velocity (b) for the steady streamers in figures 6 and 9.

With our axisymmetric model, we could not obtain steady streamers faster than  $1.2 \times 10^5$  m s<sup>-1</sup> due to streamer branching. Another limitation was the limited domain length, due to which the background electric field for the fastest two cases does not become completely constant in figure 6(b). Streamers slower than  $3 \times 10^4$  m s<sup>-1</sup> were also difficult to obtain, because the streamer velocity then becomes comparable to the ion drift velocity at the streamer head, causing the streamers to easily stagnate. However, the range of steady propagation fields in our simulations agrees well with the range of experimental stability fields (from 4.14 kV cm<sup>-1</sup> to 6 kV cm<sup>-1</sup>) in [8, 10, 11].

Our results show that the streamer stability field depends not only on the gas, but also on the streamer properties. If a faster and wider streamer is able to form, it can propagate in lower background electric fields, which could explain some of the variation in experimentally determined stability fields in air. For example, in [11] streamers were generated from a needle in a plate-plate geometry. It was found that a higher pulse voltage generated faster streamers, which required a lower background electric field to cross the gap. The minimal steady propagation field in our simulations is about 4.1 kV cm<sup>-1</sup>. This value agrees well with the lowest stability fields in air in previous experimental studies [10, 11, 13].

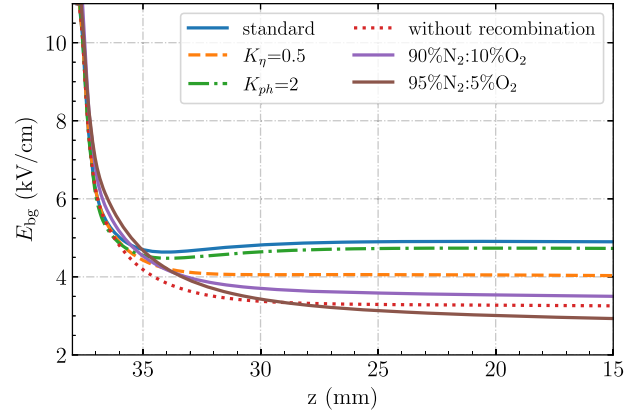


**Figure 9.** Background electric field versus streamer position for different N<sub>2</sub>-O<sub>2</sub> mixtures and for different transport data. The streamers obtain a constant velocity of  $5 \times 10^4$  m s<sup>-1</sup>. The label ‘standard’ indicates the streamer in artificial air (80% N<sub>2</sub>:20% O<sub>2</sub>). The labels ‘ $K_{\eta} = 0.5$ ’ and ‘ $K_{ph} = 2$ ’ indicate cases with half the attachment rate and double the amount of photoionization, respectively.

### 3.2. Analysis of steady streamer properties

Figure 7 shows streamer velocities, radii, maximal electric fields and background electric fields corresponding to steady propagation. Two approximately proportional relations between these variables can be observed. The ratio  $E_{max}/E_{bg}$  is about  $40 \pm 2$ , and the ratio  $R/v$  is about  $(0.95 \pm 0.2)$  ns. Below, we show how these properties can be linked by considering the electric potential difference at the streamer head  $\delta\phi$ .

First, the effective streamer length can be written as  $L_{eff} = v\tau$ , where  $\tau$  is a characteristic time scale for the loss of conductivity, see section 3.1. Just behind the streamer head, the electric field is almost fully screened, and further behind the head it relaxes back to the background field. Assuming that the relaxation occurs exponentially, with a characteristic length scale  $L_{eff}$ , the corresponding potential difference is

$$\delta\phi = v\tau E_{bg}. \quad (7)$$

Second, the electric field in the vicinity of a streamer head decays approximately quadratically, like that of a charged sphere, with the decay depending on the streamer radius. If one assumes that  $E_{bg} \ll E_{max}$ , a simple approximation is given by  $E(z) = E_{max} (1 + z/R)^{-2}$ , with  $z = 0$  corresponding to the location of  $E_{max}$  at the streamer head. Although this approximation is only justified for  $z \lesssim R$ , most of the potential drop occurs in this region. It is therefore not unreasonable to integrate up to  $\infty$ , giving

$$\delta\phi = \int_0^{\infty} E(z) dz = E_{max} R. \quad (8)$$

If equations (7) and (8) are combined, the result is

$$\tau = \frac{E_{max} R}{v E_{bg}}. \quad (9)$$

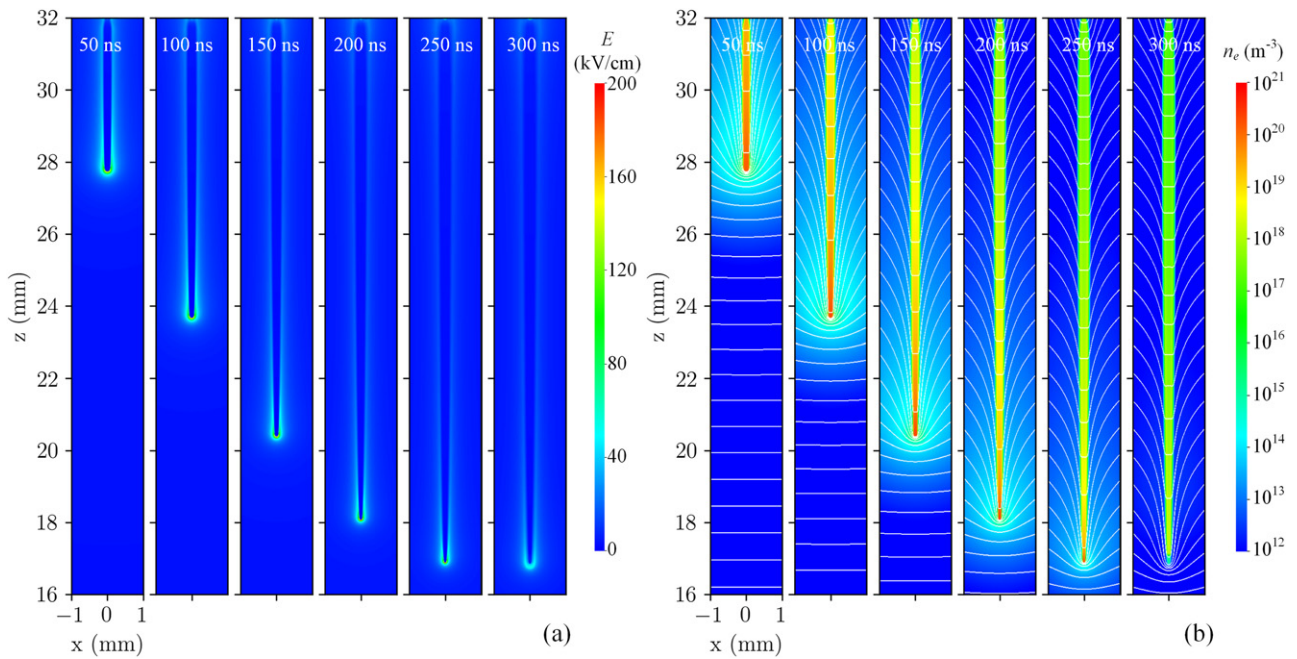


**Figure 10.** Electric field (a) and electron density (b) of the stagnating positive streamer in air with an applied voltage of 12 kV between 50 ns and 300 ns. The white equipotential lines are spaced by 240 V.

Figure 8 shows  $\tau$ , as defined by equation (9), versus the background electric field and the streamer velocity. The result lies between 33 and 49 ns, which corresponds well with the electron loss time scales due to recombination and attachment given in [15]. Variation in  $\tau$  is to be expected, because attachment and recombination rates in the streamer channel can vary, for example due to different electron density and the electric field profiles. Furthermore, equation (9) was derived based on rather simple approximations, and does for example not take the degree of ionization produced by the streamer into account.

For future analysis, we provide additional information on the steady streamers in appendix B, e.g., the maximal electron density, the maximal drift velocity and the maximal ionization rate.

### 3.3. Steady streamers in other $N_2$ - $O_2$ mixtures

In this section, we study streamers propagating at  $5 \times 10^4$  m  $s^{-1}$  in other  $N_2$ - $O_2$  mixtures, namely 90%  $N_2$ :10%  $O_2$  and 95%  $N_2$ :5%  $O_2$ , again using the velocity control method but with  $T_0 = 4$  ns. We also consider cases with modified data for air, using either half the attachment rate, double the amount of photoionization or no recombination reactions, to understand the effect of these processes on the steady propagation mode. Figure 9 shows the background electric field versus streamer position for these cases. The steady propagation fields for streamers at  $5 \times 10^4$  m  $s^{-1}$  are around 4.9 kV  $cm^{-1}$  in air, 3.5 kV  $cm^{-1}$  in 90%  $N_2$ :10%  $O_2$  and 2.9 kV  $cm^{-1}$  in 95%  $N_2$ :5%  $O_2$ .

As shown in figure 9, the effect of doubling the amount of photoionization is rather small, in agreement with e.g. [26, 44]. However, both the attachment and the recombination rate have a significant effect on the steady propagation field. This explains why steady propagation fields are lower with less  $O_2$ ,

as attachment and recombination rates are then reduced, see table 1. The dominant recombination process in our simulations is between e and  $O_4^+$ , as  $O_4^+$  is one of the main positive ions in the streamer channel [45]. With less  $O_2$ , there will also be less  $O_4^+$ .

The  $\times$ -symbols in figure 8 show the electron loss time scale  $\tau$  given by equation (9) for these steady streamers. As expected,  $\tau$  increases when the attachment rate is halved, when recombination reactions are omitted and when there is less  $O_2$ . Note that for the case  $K_\eta = 0.5$ , only the attachment rates are halved, and the recombination rates remain the same. It is therefore different from the case in 90%  $N_2$ :10%  $O_2$ , in which both attachment and recombination are reduced.

## 4. Investigation of stagnating streamers

Being able to predict whether a streamer can cross a given discharge gap is useful for many applications. In section 3 we have investigated streamers at constant velocities, which lie at the unstable boundary between acceleration and deceleration. These results help to predict whether a streamer with a certain radius and velocity will accelerate or decelerate, depending on the background field. However, streamers that decelerate might still propagate a significant distance. To predict how far they will go, we need to better understand their deceleration. In this section we therefore simulate decelerating streamers that eventually stagnate.

### 4.1. The characteristics of stagnating streamers

In this section, stagnating streamers are generated in low background fields, using constant applied voltages. To still

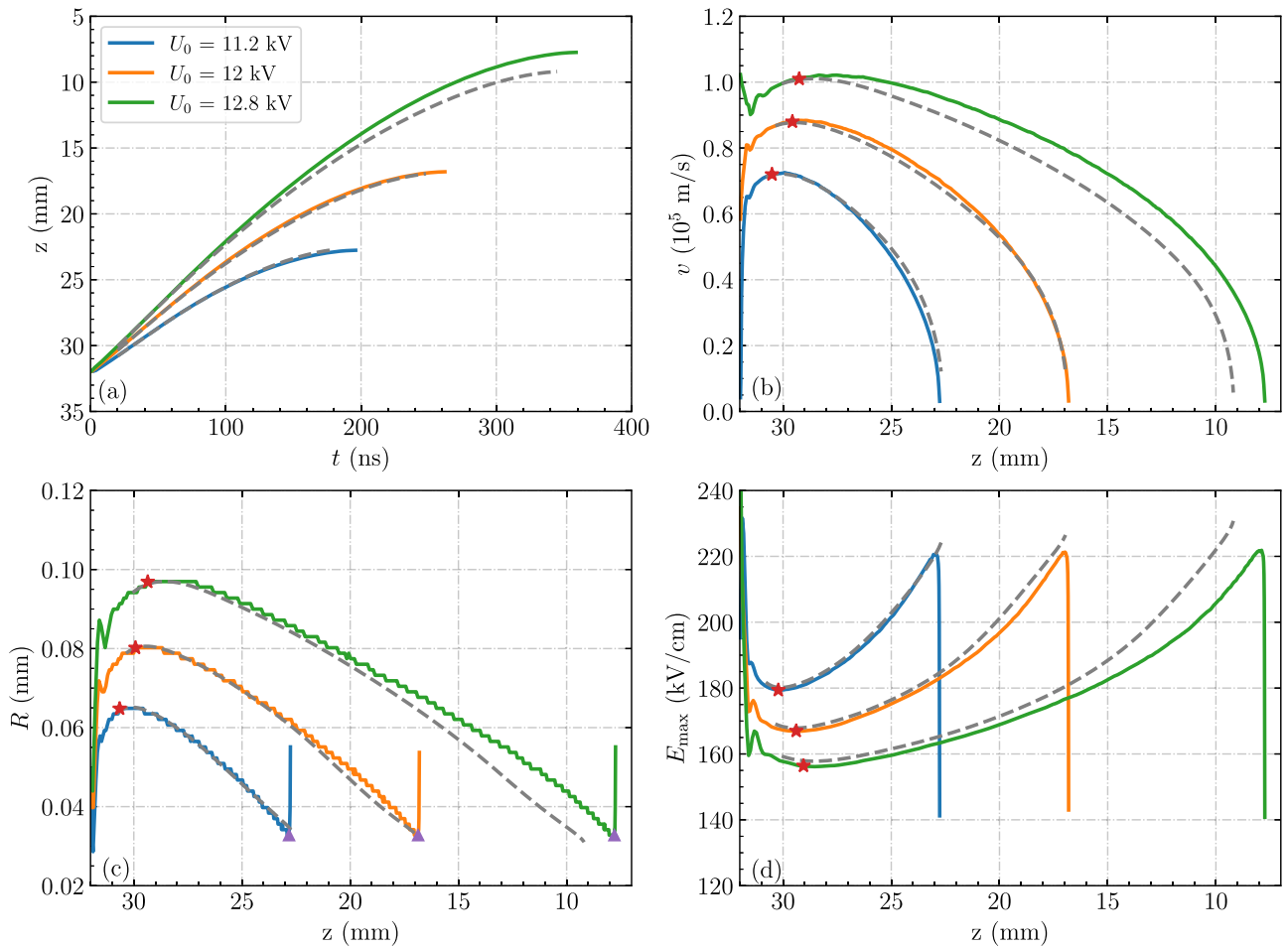


**Figure 11.** Stagnating streamers in air for applied voltages of 11.2 kV, 12 kV and 12.8 kV. (a) Position versus time, (b) streamer velocity, (c) streamer radius and (d) maximum electric field versus streamer position. The results of axisymmetric fluid simulations are indicated by solid lines. Solutions of the phenomenological model given by equation (13) are indicated by dashed lines, using  $\tau = 38.7$  ns,  $\tau_r = 2\tau$  and  $R_{\min} = 26$   $\mu\text{m}$ . The red stars indicate the locations where the background field is equal to  $E_{\text{steady}}(v)$  (panel (b)),  $E_{\text{steady}}(R)$  (panel (c)) and  $E_{\text{steady}}(E_{\max})$  (panel (d)). Here  $E_{\text{steady}}(v)$  is the background field corresponding to steady propagation as a function of  $v$  (see figure 7), and similarly so for  $E_{\text{steady}}(R)$  and  $E_{\text{steady}}(E_{\max})$ . The purple triangles indicate stagnation points.

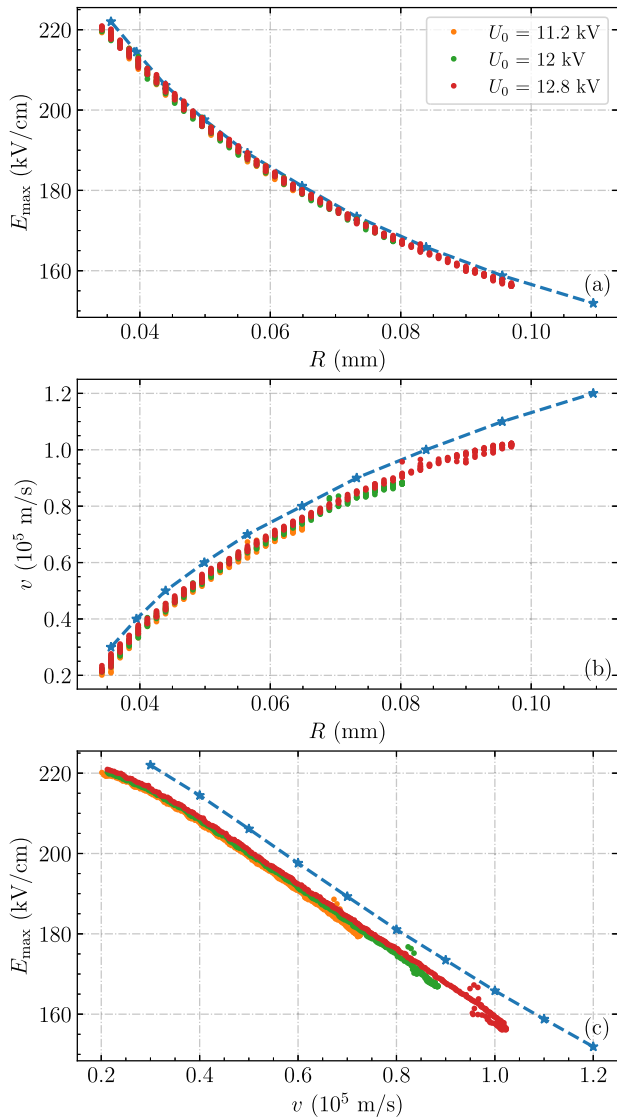
get discharge inception, a longer and sharper needle electrode is used, as described in section 2. Simulations are performed at constant applied voltages of 11.2, 12 and 12.8 kV, which correspond to background electric fields of 2.8, 3.0 and 3.2  $\text{kV cm}^{-1}$ , respectively. Figure 10 shows the discharge evolution for the 12 kV case. The streamer decelerates and becomes narrower between 50 ns and 250 ns, and it stops after about 250 ns. Note that the electric field and electron density at streamer head also decay after 250 ns, in agreement with [20].

Figure 11 shows the evolution of the streamer head position, velocity, radius and maximal electric field for the three stagnating streamers. As expected, a streamer stops earlier with a lower applied voltage. Several phases can be identified. First there is acceleration in the high field near the electrode, during which  $R$  increases and  $E_{\max}$  decreases. Then there is a transition period, after which the streamer starts to decelerate, with  $R$  decreasing and  $E_{\max}$  increasing, and the amount of charge in the streamer head decreasing. Eventually, the streamer velocity becomes similar to the ion velocity at the streamer head, and the streamer stagnates, as was also observed in [20]. The stag-

nation time and length are defined as the time and the streamer length when the radius again starts to increase, as shown in figure 11(c).

With a higher applied voltage, the radius and velocity are larger whereas  $E_{\max}$  is lower. However, the minimal streamer radii are around 32  $\mu\text{m}$  for all cases, close to the minimal steady streamer radius in figure 7.

In figure 12, we compare temporal  $v$ ,  $R$  and  $E_{\max}$  data for the stagnating streamers with data for steady states. The relations between  $v$ ,  $R$  and  $E_{\max}$  are similar, even though the stagnating streamers develop in lower background fields. For each of these quantities, the background field corresponding to steady propagation can be obtained from figure 7, so that we have functions  $E_{\text{steady}}(v)$ ,  $E_{\text{steady}}(R)$  and  $E_{\text{steady}}(E_{\max})$ . In figure 11, we have marked the locations where the actual background field is equal to  $E_{\text{steady}}(v)$ ,  $E_{\text{steady}}(R)$  and  $E_{\text{steady}}(E_{\max})$ . Note that at these locations the time derivatives of the respective quantities are approximately zero, as is the case for steady propagation. In conclusion, the results obtained for steady streamers



**Figure 12.** Data for the stagnating streamers shown in figure 11, with each data point corresponding to a different time. (a) The maximum electric field versus the streamer radius. (b) The streamer velocity versus the streamer radius. (c) The maximum electric field versus the streamer velocity. Curves for steady streamers (blue dashed lines) are shown for comparison.

can help to predict whether a streamer with given properties accelerates or decelerates, with continued deceleration leading to stagnation.

#### 4.2. A phenomenological model for stagnating streamers

The deceleration of a streamer depends on multiple properties, e.g., its current velocity, radius and the background electric field. To quantify this deceleration, we now construct a fitted model for stagnating streamers. This model is based on their similarity to the steady streamers studied in section 3, so we start from equation (9). For the data shown in figure 7,  $E_{\max}$  can empirically be expressed in terms of the streamer radius as

$$E_{\max}(R) = c_0 R^{-1/3} = 7.25 \times 10^5 \left( \frac{1 \text{ m}}{R} \right)^{1/3} \text{ V m}^{-1}, \quad (10)$$

with an error below 1%. Plugging this into equation (9) gives  $\tau = c_0 R^{2/3} / (v E_{\text{bg}})$ . Solving for  $v$  and  $R$  gives the following expressions

$$v^* = c_0 R^{2/3} / (E_{\text{bg}} \tau), \quad (11)$$

$$R^* = (E_{\text{bg}} \tau v / c_0)^{3/2}. \quad (12)$$

We know that streamers satisfying these equations, for a certain value of  $\tau$ , keep the same radius and velocity. A simple coupled differential equation that also satisfies these properties is

$$\begin{aligned} \partial_t v &= (v - v^*) / \tau_r, \\ \partial_t R &= (\max[R^*, R_{\min}] - R) / \tau_r, \end{aligned} \quad (13)$$

with  $v^*$  and  $R^*$  given as above,  $\tau_r$  a relaxation time scale and  $R_{\min}$  a minimal radius. If we fit this model to the stagnating streamer data, rather good agreement is obtained for  $\tau = 38.7$  ns,  $\tau_r = 2\tau$  and  $R_{\min} = 26 \mu\text{m}$ , which all seem reasonable. Solutions for these parameters are shown as dashed lines in figure 11. These solutions start at  $t = 20$  ns and they take the spatial dependence of the background field into account. The relatively good agreement suggests that equation (13) can be useful to describe the deceleration of a streamer.

#### 4.3. Stability field

We now consider the relation between the streamer length and the concept of a stability field. The streamer stability field is usually defined as  $E_{\text{st}} = V_0/d$ , where  $V_0$  is the applied voltage at which a streamer is just able to cross a discharge gap of width  $d$  [1, 10, 12, 13]. This concept can in principle also be applied to streamers that do not cross the gap, with a length  $L_s < d$ . A commonly used empirical equation, see e.g. [46, 47], is

$$\int_0^{L_s} (E_{\text{bg}}(z) - E_{\text{st}}) dz = 0, \quad (14)$$

where  $E_{\text{bg}}$  is the background electric field and the line from  $z = 0$  to  $z = L_s$  corresponds to the streamer's path. Equation (14) can also be written in terms of the background electric potential  $\phi_0(z)$  as  $E_{\text{st}} = (\phi_0(0) - \phi_0(L_s)) / L_s$ .

For the stagnating streamers at applied voltages of 11.2, 12.0 and 12.8 kV, the corresponding values of  $E_{\text{st}}$  are 5.18, 4.54 and 4.27 kV cm<sup>-1</sup>. These values are in the range of typical observed stability fields. For a higher applied voltage  $E_{\text{st}}$  is lower, because a faster streamer forms, in agreement with the results of section 3. By using a lower bound for  $E_{\text{st}}$ , equation (14) can give an upper bound for the streamer length. If we use  $E_{\text{st}} = 4.1$  kV cm<sup>-1</sup>, as found in section 3, the maximal lengths are 16, 21 and 27 mm for applied voltages of 11.2, 12.0 and 12.8 kV. For comparison, the actual observed lengths are 9.2, 15.1 and 24.2 mm, respectively.

The analysis above was based on the background electric field. In contrast to experimental studies, we can also determine the average electric field inside the streamer channel  $\bar{E}_{\text{ch}}$  in our simulations, including space charge effects. We measure  $\bar{E}_{\text{ch}}$  as the average field between the electrode and the location where the streamer's electric field has a maximum. In other words,  $\bar{E}_{\text{ch}} = (\phi_0(0) - \phi(z, t))/L_s$ , where  $z$  and  $t$  are the stagnation location and time, respectively. This results in average fields of 3.22, 3.36 and 3.52 kV cm<sup>-1</sup> for applied voltages of 11.2, 12.0 and 12.8 kV. These values are significantly lower than the stability fields determined above because they are based on the electrically screened part of the channel. We can relate  $\bar{E}_{\text{ch}}$  and  $E_{\text{st}}$  by considering the potential difference induced by the streamer head, here denoted as  $\delta\phi(z, t) = \phi(z, t) - \phi_0(z)$ . It then follows that

$$\delta\phi(z, t) = L_s (E_{\text{st}} - \bar{E}_{\text{ch}}). \quad (15)$$

For applied voltages of 11.2, 12.0 and 12.8 kV, the corresponding values of  $\delta\phi$  are 1.81, 1.79 and 1.80 kV. Note that when a streamer crosses a discharge gap, the head potential is zero, so that  $E_{\text{st}} = \bar{E}_{\text{ch}}$ .

In previous work  $\bar{E}_{\text{ch}}$  has been used as a measure of the stability field  $E_{\text{st}}$ , even for streamers not crossing the gap [1, 16, 48]. Our results show that  $\bar{E}_{\text{ch}}$  and  $E_{\text{st}}$  can differ significantly. However, according to equation (15)  $\bar{E}_{\text{ch}}$  and  $E_{\text{st}}$  converge for large streamer length, if one assumes a finite head potential. Finally, we remark that the value of  $\bar{E}_{\text{ch}} = (\phi_0(0) - \phi(z, t))/L_s$  depends on  $z$ . We have here used the location corresponding to the maximal electric field. Placing  $z$  behind the charge layer of the streamer head reduces  $\bar{E}_{\text{ch}}$ , whereas placing it further ahead increases  $\bar{E}_{\text{ch}}$ , due to the large field around the streamer head.

## 5. Conclusions & outlook

### 5.1. Conclusions

We have studied the properties of steady and stagnating positive streamers in air, using an axisymmetric fluid model. Streamers with constant velocities were obtained by initially adjusting the applied voltage based on the streamer velocity. Our main findings are listed below.

- Positive streamers with constant velocities between  $1.2 \times 10^5$  and  $3 \times 10^4$  m s<sup>-1</sup> could be obtained in background electric fields from 4.1 kV cm<sup>-1</sup> to 5.4 kV cm<sup>-1</sup>. This range corresponds well with experimentally determined stability fields.
- The steady streamers are not actually stable, in the sense that a small change in their properties will eventually lead to either acceleration or deceleration.
- The effective length of a streamer can be described by  $v\tau$ , where  $v$  is the streamer velocity and  $\tau$  a time scale for the loss of conductivity in the streamer channel. A faster streamer has a longer effective length, and can therefore propagate in a lower background electric field than a slower one.

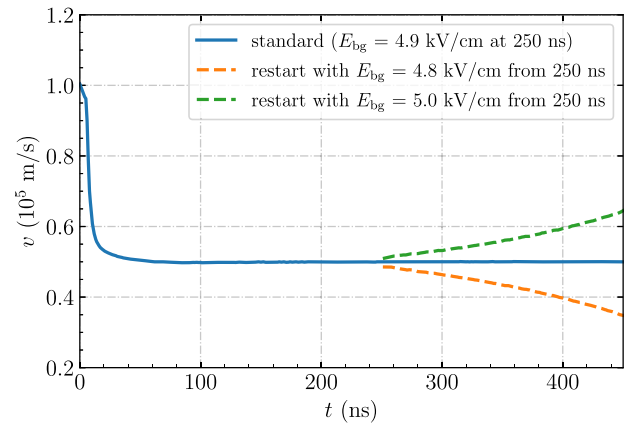


**Figure A1.** Illustration of the instability of steady positive streamers. The solid line represents a streamer whose velocity is forced to be  $5 \times 10^4$  m s<sup>-1</sup>. The dashed lines represent streamers that continued from the steady case at 250 ns in a background electric field modified by  $\pm 0.1$  kV cm<sup>-1</sup>.

- For the steady streamers, the ratio between radius and velocity is about  $R/v \sim 0.95 \pm 0.2$  ns and the ratio between the maximal field at the streamer head and the background field is about  $E_{\text{max}}/E_{\text{bg}} \sim 40 \pm 2$ . However, there is no clear linear trend between these variables. To a good approximation,  $E_{\text{max}} \propto R^{-1/3}$ .
- The radius, velocity, maximal electric field and background electric field of steady streamers can be related to the conductivity loss time scale  $\tau$  as  $\tau = RE_{\text{max}}/vE_{\text{bg}}$ . In air, the obtained values of  $\tau$  range from 33 to 49 ns.
- In N<sub>2</sub>-O<sub>2</sub> mixtures with less O<sub>2</sub> than air, steady streamers require lower background electric fields, due to reduced attachment and recombination rates that result in a longer effective length.
- By using a correction factor for the impact ionization source term and by including ion motion, it was possible to simulate stagnating streamers without an unphysical divergence in the electric field.
- If a streamer forms near a sharp electrode and then enters a low background field, it will first accelerate, then decelerate, and eventually stagnate. The transition between acceleration and deceleration occurs close to the background electric field corresponding to steady propagation. The relationships between  $v$ ,  $R$  and  $E_{\text{max}}$  for decelerating streamers are similar to those of steady streamers.
- A phenomenological model with fitted coefficients was presented to describe the velocity and radius of decelerating streamers, based on the properties of steady streamers.
- For a streamer that has stagnated, the average background electric field between the streamer head and tail resembles the empirical stability field. The average electric field inside the streamer channel can be significantly lower, in particular for relatively short streamers.

**Table B1.** Properties of the steady streamers simulated in section 3, see appendix B for a description of the columns.

Velocity (m s <sup>-1</sup> )	$E_{bg}$ (kV cm <sup>-1</sup> )	$R$ ( $\mu$ m)	$E_{max}$ (kV cm <sup>-1</sup> )	$E_{min}$ (kV cm <sup>-1</sup> )	$v_d(E_{max})$ (m s <sup>-1</sup> )	$\max(n_e)$ (m <sup>-3</sup> )	$n_\alpha(E_{max})$ (m <sup>-3</sup> )	$S(E_{max})$ (s <sup>-1</sup> )	$\delta\phi$ (kV)
$3 \times 10^4$	5.42	36	222	0.42	$6.1 \times 10^5$	$3.12 \times 10^{20}$	$1.68 \times 10^{20}$	$2.24 \times 10^{11}$	1.52
$4 \times 10^4$	5.10	40	214	0.50	$5.9 \times 10^5$	$2.94 \times 10^{20}$	$1.53 \times 10^{20}$	$2.09 \times 10^{11}$	1.61
$5 \times 10^4$	4.86	44	206	0.56	$5.8 \times 10^5$	$2.70 \times 10^{20}$	$1.38 \times 10^{20}$	$1.93 \times 10^{11}$	1.72
$6 \times 10^4$	4.65	50	197	0.66	$5.6 \times 10^5$	$2.43 \times 10^{20}$	$1.22 \times 10^{20}$	$1.77 \times 10^{11}$	1.84
$7 \times 10^4$	4.47	57	189	0.74	$5.4 \times 10^5$	$2.16 \times 10^{20}$	$1.08 \times 10^{20}$	$1.61 \times 10^{11}$	1.97
$8 \times 10^4$	4.33	65	181	0.82	$5.3 \times 10^5$	$1.90 \times 10^{20}$	$9.53 \times 10^{19}$	$1.46 \times 10^{11}$	2.12
$9 \times 10^4$	4.22	73	173	0.94	$5.1 \times 10^5$	$1.68 \times 10^{20}$	$8.40 \times 10^{19}$	$1.33 \times 10^{11}$	2.29
$1 \times 10^5$	4.15	84	166	1.01	$5.0 \times 10^5$	$1.46 \times 10^{20}$	$7.35 \times 10^{19}$	$1.20 \times 10^{11}$	2.46
$1.1 \times 10^5$	4.09	96	159	1.08	$4.8 \times 10^5$	$1.28 \times 10^{20}$	$6.44 \times 10^{19}$	$1.09 \times 10^{11}$	2.64
$1.2 \times 10^5$	4.05	110	152	1.17	$4.7 \times 10^5$	$1.11 \times 10^{20}$	$5.61 \times 10^{19}$	$9.76 \times 10^{10}$	2.83

## 5.2. Outlook

In future work, it would be interesting to include streamer branching and to study the propagation of multiple interacting streamers. For example, it could be possible that due to repeated branching, streamers in moderately high background field will not continually accelerate, but on average obtain a certain velocity and radius. Another interesting aspect is how the presence of multiple streamers changes the background field required for their collective propagation, i.e., the stability field.

## Acknowledgments

XL was supported by STW-project 15052 ‘Let CO<sub>2</sub> Spark’ and the National Natural Science Foundation of China (Grant No. 52077169). BG was funded by the China Scholarship Council (CSC) (Grant No. 201906280436). We acknowledge Hani Francisco for valuable discussions.

## Data availability statement

The data that support the findings of this study are openly available at the following URL/DOI: <https://doi.org/10.5281/zenodo.5873579>.

## Appendix A. Instability of steady positive streamers

We here illustrate the instability of steady positive streamers. First, a streamer whose velocity is forced to be  $5 \times 10^4$  m s<sup>-1</sup>. At 250 ns, it reaches a steady state with a  $E_{bg}$  of 4.9 kV cm<sup>-1</sup>. We use this steady state as the initial condition and restart the simulation with  $E_{bg}$  modified by  $\pm 0.1$  kV cm<sup>-1</sup>. Figure A1 shows that the streamer velocity then differs about 30% after 200 ns.

Similar behavior was previously found in [15] for positive streamers and in [49] for steady negative streamers.

## Appendix B. Additional information on steady streamers

For future analysis, table B1 provides additional properties of the steady streamers simulated in section 3. All these values are measured at the moments corresponding to figure 4. The table contains the following columns:

- $E_{bg}$  is the steady propagation field
- $R$  is the streamer radius, measured as the radius where the radial electric field has a maximum
- $E_{max}$  is the maximal electric field
- $E_{min}$  is the minimal electric field in the streamer channel, just behind the streamer head
- $v_d(E_{max})$  is the electron drift velocity corresponding to  $E_{max}$
- $\max(n_e)$  is the maximum electron density around the streamer head
- $n_\alpha(E_{max})$  is an approximate relation between the maximal electric field and the degree of ionization in the streamer channel [50, 51], given by

$$n_\alpha(E_{max}) = \frac{\epsilon_0}{e} \int_0^{E_{max}} \alpha_{eff}(E) dE, \quad (B.1)$$

where  $\alpha_{eff}$  is the effective ionization coefficient. For positive streamers,  $n_\alpha(E_{max})$  has been observed to be about half the degree of ionization in the channel [1].

- $S(E_{max})$  is the ionization rate corresponding to  $E_{max}$
- $\delta\phi$  is the potential difference at the streamer head, defined as  $\phi(z, t) - \phi_0(z)$ , with  $z$  the location corresponding to  $E_{max}$ .

## ORCID iDs

Xiaoran Li  <https://orcid.org/0000-0003-3354-9078>  
 Baohong Guo  <https://orcid.org/0000-0001-8368-5014>  
 Anbang Sun  <https://orcid.org/0000-0003-1918-3110>  
 Ute Ebert  <https://orcid.org/0000-0003-3891-6869>  
 Jannis Teunissen  <https://orcid.org/0000-0003-0811-5091>

## References

- [1] Nijdam S, Teunissen J and Ebert U 2020 *Plasma Sources Sci. Technol.* **29** 103001
- [2] Ebert U, Nijdam S, Li C, Luque A, Briels T and van Veldhuizen E 2010 *J. Geophys. Res.: Space Phys.* **115** A00E43
- [3] Weltmann K D et al 2019 *Plasma Process. Polym.* **16** 1800118
- [4] Bárδος L and Baránková H 2010 *Thin Solid Films* **518** 6705–13
- [5] Laroussi M 2014 *Plasma Process. Polym.* **11** 1138–41
- [6] Popov N A 2016 *Plasma Sources Sci. Technol.* **25** 043002
- [7] Gallimberti I 1979 *J. Phys. Colloq.* **40** C7-193–250
- [8] Phelps C T 1971 *J. Geophys. Res.* **76** 5799–806
- [9] Griffiths R F and Phelps C T 1976 *Q. J. R. Meteorol. Soc.* **102** 419–26
- [10] Allen N L and Boutlind M 1991 *IEE Proc. A Sci. Meas. Technol. UK* **138** 37
- [11] Allen N L and Ghaffar A 1995 *J. Phys. D: Appl. Phys.* **28** 331–7
- [12] van Veldhuizen E M and Rutgers W R 2002 *J. Phys. D: Appl. Phys.* **35** 2169–79
- [13] Seeger M, Votteler T, Ekeberg J, Pancheshnyi S and Sánchez L 2018 *IEEE Trans. Dielect. Electr. Insul.* **25** 2147–56
- [14] Qin J and Pasko V P 2014 *J. Phys. D: Appl. Phys.* **47** 435202
- [15] Francisco H, Teunissen J, Bagheri B and Ebert U 2021 *Plasma Sources Sci. Technol.* **30** 115007
- [16] Briels T M P, Kos J, Winands G J J, van Veldhuizen E M and Ebert U 2008 *J. Phys. D: Appl. Phys.* **41** 234004
- [17] Raizer Y P 1991 *Gas Discharge Physics* (Berlin: Springer)
- [18] Pancheshnyi S V and Starikovskii A Y 2004 *Plasma Sources Sci. Technol.* **13** B1–5
- [19] Starikovskiy A Y, Aleksandrov N L and Shneider M N 2021 *J. Appl. Phys.* **129** 063301
- [20] Niknezhad M, Chanrion O, Holbøll J and Neubert T 2021 *Plasma Sources Sci. Technol.* **30** 105001
- [21] Soloviev V R and Krivtsov V M 2009 *J. Phys. D: Appl. Phys.* **42** 125208
- [22] Teunissen J 2020 *Plasma Sources Sci. Technol.* **29** 015010
- [23] Luque A, Ratushnaya V and Ebert U 2008 *J. Phys. D: Appl. Phys.* **41** 234005
- [24] Naidis G V 2009 *Phys. Rev. E* **79** 1550–2376
- [25] Teunissen J and Ebert U 2017 *J. Phys. D: Appl. Phys.* **50** 474001
- [26] Li X, Dijkstra S, Nijdam S, Sun A, Ebert U and Teunissen J 2021 *Plasma Sources Sci. Technol.* **30** 095002
- [27] Bagheri B et al 2018 *Plasma Sources Sci. Technol.* **27** 095002
- [28] Wang Z, Sun A and Teunissen J 2022 *Plasma Sources Sci. Technol.* **31** 015012
- [29] Zheleznyak M, Mnatsakanyan A and Sizykh S 1982 *High Temp.* **20** 357–62
- [30] Luque A, Ebert U, Montijn C and Hundsdoerfer W 2007 *Appl. Phys. Lett.* **90** 081501
- [31] Bourdon A, Pasko V P, Liu N Y, Célestin S, Ségur P and Marode E 2007 *Plasma Sources Sci. Technol.* **16** 656–78
- [32] Hagelaar G J M and Pitchford L C 2005 *Plasma Sources Sci. Technol.* **14** 722–33
- [33] Phelps A V and Pitchford L C 1985 *Phys. Rev. A* **31** 2932–49
- [34] Phelps database (N<sub>2</sub>, O<sub>2</sub>) [www.lxcat.net](http://www.lxcat.net) retrieved on (19 January 2021)
- [35] Tochikubo F and Arai H 2002 *Japan. J. Appl. Phys.* **41** 844
- [36] Naidis G V 1997 *Tech. Phys. Lett.* **23** 493–4
- [37] Li C, Ebert U and Hundsdoerfer W 2010 *J. Comput. Phys.* **229** 200–20
- [38] Kossyi I A, Kostinsky A Y, Matveyev A A and Silakov V P 1992 *Plasma Sources Sci. Technol.* **1** 207–20
- [39] Pancheshnyi S 2013 *J. Phys. D: Appl. Phys.* **46** 155201
- [40] Aleksandrov N L and Bazelyan E M 1999 *Plasma Sources Sci. Technol.* **8** 285–94
- [41] Teunissen J and Ebert U 2018 *Comput. Phys. Commun.* **233** 156–66
- [42] Teunissen J and Schiavello F 2022 arXiv:2205.09411
- [43] Pancheshnyi S, Nudnova M and Starikovskii A 2005 *Phys. Rev. E* **71** 1550–2376
- [44] Bagheri B and Teunissen J 2019 *Plasma Sources Sci. Technol.* **28** 045013
- [45] Nijdam S, Takahashi E, Markosyan A H and Ebert U 2014 *Plasma Sources Sci. Technol.* **23** 025008
- [46] Seeger M, Avaheden J, Pancheshnyi S and Votteler T 2016 *J. Phys. D: Appl. Phys.* **50** 015207
- [47] Bujotzek M, Seeger M, Schmidt F, Koch M and Franck C 2015 *J. Phys. D: Appl. Phys.* **48** 245201
- [48] Morrow R and Lowke J J 1997 *J. Phys. D: Appl. Phys.* **30** 614–27
- [49] Guo B, Li X, Ebert U and Teunissen J 2022 arXiv:2204.02698
- [50] Ebert U, van Saarloos W and Caroli C 1996 *Phys. Rev. Lett.* **77** 4178–81
- [51] Babaeva N Y and Naidis G V 1996 *J. Phys. D: Appl. Phys.* **29** 2423–31